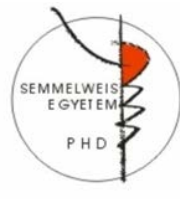


The application of nonlinear microscopy techniques in  
the assessment of skin tumors and hereditary skin  
disorders

Doctoral theses

**Norbert Ferenc Kiss, MD**

Semmelweis University  
Doctoral School of Clinical Medicine



**Supervisor:** Prof. Norbert Wikonkál, MD, PhD, DSc  
**Consultant:** Róbert Szipőcs, PhD

**Official reviewers:**

Krisztián Gáspár, MD, PhD  
Gusztáv Schay, PhD

**Head of the Complex Examination Committee:**

Prof. Anikó Somogyi, MD, PhD, DSc

**Head of the Complex Examination Committee:**

Prof. Szalai Zsuzsanna, MD, PhD  
Tibor Krenács, PharmD, PhD, DSc

Budapest  
2019

## **Introduction**

Novel imaging techniques have been a great development for various fields of medicine and now they are widely integrated into everyday clinical practice. These techniques have revolutionized medical diagnostics and they became essential for both therapy monitoring and clinical research.

In the last decades, nonlinear optical methods have undergone significant developments, which led to their application as novel, non-invasive imaging techniques with very high tissue resolution. Nonlinear optics describes the behavior of light in special media where polarization ( $P$ ) depends nonlinearly on the electric field of light ( $E$ ). Nonlinear optical microscopic modalities can be classified based on the number of the required laser beams for their generation. One-beam modalities include two-photon absorption fluorescence (TPF) and second-harmonic generation (SHG). Two beams are needed for coherent anti-Stokes Raman scattering, CARS. Different nonlinear optical methods are able to provide 3D optical biopsies of the skin with high spatial and temporal resolution. Moreover, nonlinear microscopy is capable of *in vivo* stain-free histologic assessment of the skin. In addition, utilizing various nonlinear optical methods, different components of the skin can be selectively visualized, providing multimodal imaging.

## **Aims**

### ***I. experiment***

In the first experiment, our aim was to apply nonlinear microscopy as an imaging method with higher diagnostic accuracy than present techniques for the diagnosis of skin cancer, including basal cell carcinoma (BCC). In our first experiment, we aimed to introduce various quantifiable parameters using for the diagnosis of BCC during nonlinear optical imaging. We carried out TPF and SHG microscopic measurements on *ex vivo* BCC samples and healthy control skin. We utilized different image processing and image analysis methods to identify such parameters which show significant difference in BCC samples compared to healthy skin. These parameters could be used for the surgical planning before the excision of BCC in the future.

### ***II. experiment***

In addition to the assessment of tumor borders there is an unmet clinical need for the accurate non-invasive diagnostics of the different types of skin cancer. In our second experiment, we upgraded our custom-built CARS imaging system to perform stain-free histopathologic assessments of BCC. Our further aim was to differentiate different components of tissue in the captured images with high contrast to carry out histopathologic evaluation based on morphology similar to the reading of hematoxylin and eosin (H&E) stained sections. To achieve this aim, we developed a novel image

processing algorithm to improve chemical selectivity of this technique.

### ***III. experiment***

Previously, different hereditary connective tissue disorders, including osteogenesis imperfecta and pseudoxanthoma elasticum were assessed by certain research groups using nonlinear optical imaging. Hence, the morphologic characteristics of Ehlers–Danlos syndrome (EDS) have not yet been investigated by nonlinear microscopy. As there is a niche in objective diagnostic techniques of EDS, a novel objective method in the assessment of this disorder would harbor great clinical significance. Thus, in our third experiment, our aim was to compare the collagen structure of patients with classic (cEDS) and vascular type (vEDS) EDS with healthy skin using *ex vivo* nonlinear microscopy imaging. These experiments could serve as a basis for future studies investigating the applicability of nonlinear optical techniques for the monitoring of the skin status of EDS patients and to predict clinical outcomes.

## **Methods**

### ***Skin samples***

#### ***I. experiment***

We have collected 10 nodular type BCC and healthy skin samples by surgical excision at the Department of Dermatology, Dermatocology and

Venerology, Semmelweis University. The histologic diagnosis of BCC was carried out by an expert dermatopathologist for each sample. The number of the ethical approval for the I. and II. experiment is SE TUKÉB 114/2017.

### *II. experiment*

We have anesthetized two healthy 8-week old BALB/c mice, removed the hair from their back and excised two 2x2 cm size skin samples from their upper back. In addition, we carried out the surgical excision of two infiltrative type BCC and the healthy skin samples at our department for this experiment.

### *III. experiment*

We have collected skin biopsies from three female patients with EDS (mean age:  $45 \pm 7$  years) and two age-matched healthy female volunteers who served as controls. For the histopathological evaluations, H&E, Van Gieson- (VG), and Weigert's elastic (WE) stainings were prepared at our histology laboratory. The number of the ethical approval for the III. experiment is SE TUKÉB 266/2015.

## ***Ex vivo nonlinear microscopy setting***

### *I. and III. experiment*

Nonlinear microscopy measurements were carried out in the Wigner RCP Nonlinear Microscopy Laboratory. For TPF and SHG measurements, a widely tunable femtosecond pulse Ti:sapphire laser (*FemtoRose 100TUN*

*NoTouch*, R&D Ultrafast Lasers Ltd, Budapest, Hungary) was employed with a  $\sim 796$  nm central excitation wavelength. A 460/50 nm bandwidth emission filter was used to separate TPF signal, while for SHG imaging, a 405/20 nm filter was used.

## *II. experiment*

For CARS measurements, the same Ti:sapphire laser utilized for the I. and III. experiments was used as a pump laser ( $\omega_p$ ). To generate CARS signal, a further pulse laser, an Yb fiber amplifier working on 1030 nm as a “Stokes laser” ( $\omega_s$ , *CARS Stokes Unit*, R&D Ultrafast Lasers Ltd), and also a *FemtoCARS Laser Unit-ot* (R&D Ultrafast Lasers Ltd) regulating the output, polarization, pulse length and delay of the lasers was employed. If the pulse lengths and frequency delays of the two lasers are correctly set, and the difference of the frequency of the two lasers is equal with the resonance frequency ( $\Omega = \omega_p - \omega_s$ ) of the excited molecule and anti-Stokes signal is generated deriving from the excited chemical band at the focus spot of the microscope objective with a frequency of  $\omega_{as} = 2\omega_p - \omega_s$

In the II. experiment, we optimized our CARS imaging for stain free histopathological examinations. Due to the partial overlap of the excitation spectra and the 5-6 nm typical spectral bandwidth of our lasers, we set the wavelengths for 790 nm (“proteins”) and 800 nm (“lipids”) for dual vibration resonance frequency (DVRF) CARS measurements. An additional factor, nonresonant background further decreases the chemical selectivity of

the DVRF measurements. During the image processing of our DVRF CARS images captured at 790 nm and 800 nm using ImageJ software we could substantially increase the chemical selectivity if we subtracted the two images from each other. As a result, we generated two images, a “lipid” and a “protein” image. Before the subtractions to acquire the final images, we set multiplication factors typically between 0,9-1,1 to minimize non-specific CARS and autofluorescence background.

### ***Image processing and image analysis methods***

#### ***I. experiment***

The TPF signal of NADH and elastin and the SHG signal of collagen from each field of view was converted to integrated optical density (IOD) by ImageJ software to measure the signal intensities.

We applied fast Fourier transformation (FFT) on the SHG and TPF images and converted the output images to power plots. We set ellipses to the power plots and calculated their eccentricity to acquire the collagen orientation index (COI) values. COI values close to 0 reflects the collagen structure of healthy skin, while COI close to 1 shows parallelly oriented collagen fibers. Collagen bundle packing (CBP) correlates with the periodicity of collagen fibers (the distance of the individual fibers). CBP can be calculated by  $CPB = 512 \cdot (1/h)$  where  $h$  is the measured distance of the two first-order maxima of the histogram of the FFT output images. FFT image processing and analyses were carried out using ImageJ software.

Curvelet transform and fiber extraction (CT-FIRE) and CurveAlign algorithms (Laboratory for Optical and Computational Instrumentation, Wisconsin-Madison University, Madison, Wisconsin, USA) are Curvelet-based frameworks which are developed for the analysis of collagen structure.

We customized CT-FIRE (v1.3) and CurveAlign (v4.0) algorithms for the assessment of BCC and healthy skin samples on raw SHG images. We calculated the following parameters: collagen fibers length, angle, width, straightness (CT-FIRE); orientation and alignment (CurveAlign).

Statistical analyses were carried out using GraphPad Prism v6.0 (GraphPad Software Inc., La Jolla, California, USA) software. Student's t test was used to compare the data of BCC and healthy samples after confirming normal distribution by F-test. Results were considered significant if p value was  $< 0,05$ .

## *II. experiment*

We evaluated the images based on morphologic characteristics.

## *III. experiment*

The amount of collagen and elastin was calculated by IOD measurements based on SHG and TPF signals, respectively, using ImageJ software.



## **Results**

### **I. experiment**

In the first experiment, the IOD values of SHG and TPF signals were both significantly lower in BCC compared to healthy skin samples. It could be observed that where tumor cells were present in the dermis SHG signal was not generated, only in the tumor stroma and in the surrounding dermis. The NADH signal of tumor cells also showed significantly lower signal intensities, when compared to the TPF signal of elastin fibers in the healthy dermis.

FFT transformed SHG images of BCC samples showed significantly higher COI compared to control samples. This suggest that in BCC collagen fibers are less randomly organized than in healthy skin. On the other hand, we did not find significant differences in the CPB values, thus the density of collagen fibers does not show alterations, only their orientation.

Individual collagen fiber analyses by CT-FIRE algorithm found significantly longer collagen fibers and smaller fiber angle in BCC samples compared to control skin. Whereas, the width and straightness of collagen fibers, CT-FIRE could not identify differences between BCC and normal skin.

CurveAlign software detected significantly higher collagen fiber alignment coefficient in BCC compared to healthy skin. Collagen fiber orientation values showed very high standard deviation in BCC samples and in this parameter no significant difference was found between BCC and normal skin samples.

## **II. experiment**

We captured a high number of *ex-vivo* DVRF CARS images of healthy mouse and human skin and also BCC samples. We generated pseudo H&E “stained” images using two different image processing algorithms on the “lipid” and “protein” images. We detected significant differences between the images of the CH<sub>3</sub> and CH<sub>2</sub> wavelength settings. The nuclei of the keratinocytes were clearly distinguishable on the output images using our own image processing algorithm.

In the healthy human skin samples, the dermis mainly displays a collagen-rich connective tissue when imaged by DVRF CARS technique. The BCC samples showed irregularly shaped and sized tumor nests, which were surrounded by the collagen fibers of the tumor stroma. This morphology is characteristic for infiltrative type BCC, which was also verified by conventional histopathological evaluation.

## **III. experiment**

Skin samples of the EDS patients showed an irregular, partially fragmented, loose collagen structure. Particularly in the vEDS patients, the loose collagen bands with various sizes and shapes show a disorganized appearance. In the dermis of the cEDS patient thicker collagen bands are also present, which are surrounded by fragmented collagen fibers which appear similar to the collagen fibers

in the dermis of the vEDS patients. IOD, which correlates with the amount of unimpaired collagen, is remarkably higher in the control skin compared to the EDS patients. On the other hand, the elastin content of the dermis is similar in the control skin and the skin of the vEDS patient with almost equal IOD values. However, a statistical comparison could not be made due to the low number of patients.

## **Conclusions**

### ***I. experiment***

In this experiment, we detected significantly lower IOD values of TPF and SHG signals in the BCC samples compared to controls. Yet, we consider IOD measurements as a parameter less ideal for standardization, as its value depends on various external factors. These include the excitation intensity, the depth of the imaging, and the thickness of the epidermis. On the other hand, collagen morphology analysis based on SHG images is independent from these factors.

FFT analysis of the SHG images of the collagen structure revealed significantly higher COI value in BCC compared to healthy skin, while CPB did not show alterations. Based on this data, we conclude, that in BCC the collagen structure is less randomly organized than in healthy skin. Nevertheless, we did not find notable differences in the in the density of the collagen fibers.

CT-FIRE and CurveAlign analysis of the SHG images of collagen, in BCC, collagen fibers were

significantly longer and had a lower fiber angle. In addition, collagen fiber alignment coefficient was significantly higher in BCC. The width and straightness of collagen fibers did not show an abnormality. Collagen fiber orientation showed a high standard deviation in BCC. The measurement of COI seems to be a more sensitive method for the assessment of collagen fiber orientation than CurveAlign software.

Our experiment confirms those previous studies which describe remarkable alterations of collagen structure pattern in BCC. Based on our results, *in vivo* SHG imaging may be capable of the detection of the borders of BCC. Based on the changes of the collagen structure, machine learning based automatized algorithms could be used to plan surgical borders before and during the surgical removal of BCC in the future.

## ***II. experiment***

In our second experiment, we carried out *ex vivo* DVRF CARS imaging in our custom-built CARS system. In its present form, this system is capable of *ex vivo* investigations, but following further upgrades, DVRF CARS technique could be employed also in handheld nonlinear microscopy devices.

Based on our experiments we verified, that the DVRF CARS imaging method is capable of the generation of pseudo H&E “stained” images of mice and human skin and also BCC for histopathologic evaluation.

Using a novel image processing algorithm for DVRF CARS we could increase chemical selectivity of

this method and also decrease the nonresonant background of water molecules.

### ***III. experiment***

To our best knowledge, we were the first to apply nonlinear microscopic methods in the visualization of the connective tissue morphology of the skin of patients with EDS. Using SHG method, we detected irregular, fragmented, loose collagen structure in EDS compared to healthy skin. These changes were more pronounced in the skin of vEDS patients than in cEDS. Correspondingly, IOD values of the SHG signal was lower in EDS compared to control skin, especially in vEDS. In accordance with our hypothesis, TPF method did not reveal alterations in the elastin structure of EDS patients compared to controls and also their IOD values were similar. We validated and compared our results with the evaluation of conventional histologic stains, including H&E, VG and VE stainings. We concluded, that nonlinear microscopy techniques are capable of the detection of connective tissue alterations in the skin of EDS patients.

In the background of vEDS we identified a previously not published heterozygote *COL3A1* gene variant, the c.3124\_3141dup (p.Ala1042\_Gly1047dup) mutation, which is probably pathogen, as it is predicted to alter the Gly-X-Y repeat.

Based on our experiments, *in vivo* nonlinear microscopy imaging could be used for the monitoring of the skin status of EDS-affected patients. Also, as there is a niche of widely applicable, objective non-invasive

diagnostic techniques of EDS, thus nonlinear microscopy could be included in the diagnostic scheme of EDS in the future. Further research could investigate, if the monitoring of the skin status of EDS patients using nonlinear microscopy would be beneficial for the prediction of clinical outcomes.

## List of publications

*Publications related to the dissertation:*

Kiss N, Krolopp Á, Lőrincz K, Bánvölgyi A, Szipőcs R, Wikonkál N.

Stain-free Histopathology of Basal Cell Carcinoma by Dual Vibration Resonance Frequency CARS Microscopy

***PATHOLOGY AND ONCOLOGY***

***RESEARCH*** 24(4):927-930 (2018) **IF: 1,935**

Kiss N, Haluszka D, Lőrincz K, Kuroli E, Hársing J, Mayer B, Kárpáti S, Fekete G, Szipőcs R, Wikonkál N, Medvecz M.

Ex vivo nonlinear microscopy imaging of Ehlers–Danlos syndrome-affected skin

***ARCHIVES OF DERMATOLOGICAL***

***RESEARCH*** 310(5):463-473. (2018) **IF: 2,148**

Kiss N, Haluszka D, Lőrincz K, Gyöngyösi N, Bozsányi Sz, Bánvölgyi A, Szipőcs R, Wikonkál N.

Quantitative Analysis on Ex Vivo Nonlinear Microscopy Images of Basal Cell Carcinoma Samples in Comparison to Healthy Skin

***PATHOLOGY AND ONCOLOGY RESEARCH***

doi.org/10.1007/s12253-018-0445-1 (2018)

**IF: 1,935**

*Publications not related to the dissertation:*

Bánvölgyi A, Anker P, Lőrincz K, Kiss N, Márton D, Fésűs L, Gyöngyösi N, Wikonkál N.

Smoothened Receptor Inhibitor Vismodegib for the Treatment of Basal Cell Carcinoma: a Retrospective Analysis of Efficacy and Side Effects

***JOURNAL OF DERMATOLOGICAL TREATMENT***

doi.org/10.1080/09546634.2019.1601155 (2019) **IF: 2,144**

Kiss N, Avcı P, Bánvölgyi A, Lőrincz K, Szakonyi J, Gyöngyösi N, Fésűs L, Lee G, Wikonkál N.

Intralesional therapy for the treatment of keratoacanthoma.

***DERMATOLOGIC THERAPY***. 13:12872. (2019) **IF: 1,563**

Kiss N, Anker P, Fésűs L, Lőrincz K, Bánvölgyi A, Bozsányi Sz, Wikonkál N.

A rosszindulatú hámeredetű bőrdaganatok kialakulásának genetikai háttere, új ismeretek a karcinogenezis folyamatában

***BŐRGYÓGYÁSZATI ÉS VENEROLÓGIAI SZEMLE***  
94(5):220-226. (2018)

Bánvölgyi A, Lőrincz K, Kiss N, Avcı P, Fésűs L, Szipócs R, Krenács T, Gyöngyösi N, Wikonkál N, Kárpáti S, Németh K.



Efficiency of long-term high-dose intravenous ascorbic acid therapy in locally advanced basal cell carcinoma – a pilot study

***ADVANCES IN DERMATOLOGY AND***

***ALLERGOLOGY*** doi.org/10.5114/ada.2019.83027.

(2019) **IF: 1,471**

Kiss N, Plázár D, Lőrincz K, Bánvölgyi A, Valent S, Wikonkál N.

Gynecological aspects of hidradenitis suppurativa.

***ORVOSI HETILAP*** 160(8):291-299. (2019) **IF: 0,322**

Ralovich FV, Kiss N, Horváth K, Kárpáti S, Medvecz M.

Az Ehlers–Danlos-szindrómák korszerű osztályozása és multidiszciplináris tünettana

***ORVOSI HETILAP*** 160(16):603–612. (2019) **IF: 0,322**

Róbert L, Kiss N, Medvecz M, Kuroli E, Sárdy M, Hidvégi, B.

Epidemiology and Treatment of Calcinosis Cutis: 13 Years of Experience

***INDIAN JOURNAL OF DERMATOLOGY*** In press

(2019) **IF: 1,338**

Oláh J, Varga A, Csányi I, Emri G, Kiss N, Varga E, Németh IB, Lengyel Zs, Holló P.

A rosszindulatú hámeredetű bőrdaganatok klinikai jellemzői és diagnosztikája 2018-ban

***BŐRGYÓGYÁSZATI ÉS VENEROLÓGIAI SZEMLE***

94(5):227-236. (2018)

Lőrincz K, Medvecz M, Kiss N, Glász-Bóna, Hársing J, Lepesi-Benkő R, Hatvani Z, Mazán, Kárpáti, Wikonkál N.

Confirmation of the role of a KRT5 mutation and successful management of skin lesions in a patient with Galli-Galli disease

***CLINICAL AND EXPERIMENTAL***

***DERMATOLOGY* 2018: 43(8):972-974. (2018) IF: 1,484**

Lorincz K, Haluszka D, Kiss N, Gyongyosi N, Banvolgyi A, Szipocs R, Wikonkal NM.

Voluntary exercise improves murine dermal connective tissue status in high-fat diet-induced obesity.

***ARCHIVES OF DERMATOLOGICAL***

***RESEARCH* 309(3):209-215 (2017) IF: 2,148**

Haluszka D, Lőrincz K, Kiss N, Szipőcs R, Kuroli E, Gyöngyösi N, Wikonkál NM.

Diet-induced obesity skin changes monitored by in vivo SHG and ex vivo CARS microscopy ***BIOMEDICAL***

***OPTICS EXPRESS* 7(11):4480-4489. (2016) IF: 3,337**

Lőrincz K, Kiss N, Gyöngyösi N, Wikonkál NM.

Hidradenitis suppurativa, az újra felfedezett betegség

***BŐRGYÓGYÁSZATI ÉS VENEROLÓGIAI***

***SZEMLE* 92(5):209-213. (2016)**

Kaucsar T, Godo M, Revesz C, Kovacs M, Mocsai A, Kiss N, Albert M, Krenacs T, Szenasi G, Hamar P. Urine/Plasma Neutrophil Gelatinase Associated Lipocalin Ratio Is a Sensitive and Specific Marker of Subclinical Acute Kidney Injury in Mice  
***PLOS ONE*** 11(1):0148043. (2016) **IF: 2,806**

Kiss N, Wikonkál NM.

A rosacea szisztémás kezelése  
***BŐRGYÓGYÁSZATI ÉS VENEROLÓGIAI SZEMLE*** 92(4):183-186. (2016)

Kiss N, Hamar P.

Histopathological Evaluation of Contrast-Induced Acute Kidney Injury Rodent Models  
***BIOMED RESEARCH INTERNATIONAL*** 2016:3763250. (2016) **IF: 2,476**

Szalay CI, Erdelyi K, Kokeny G, Lajtar E, Godo M, Revesz C, Kaucsar T, Kiss N, Sarkozy M, Csont T, Krenacs T, Szenasi G, Pacher P, Hamar P. Oxidative/Nitrative Stress and Inflammation Drive Progression of Doxorubicin-Induced Renal Fibrosis in Rats as Revealed by Comparing a Normal and a Fibrosis-Resistant Rat Strain  
***PLOS ONE*** 10(6):0127090. (2015) **IF: 3,057**